

# Observation of inter-layer charge transmission resonance at optically excited graphene–TMDC interfaces

Cite as: APL Mater. 8, 091114 (2020); <https://doi.org/10.1063/5.0020396>

Submitted: 01 July 2020 • Accepted: 31 August 2020 • Published Online: 22 September 2020

 Ranjit Kashid, Jayanta Kumar Mishra,  Avradip Pradhan, et al.

## COLLECTIONS

Paper published as part of the special topic on [Moire Materials](#)



View Online



Export Citation



CrossMark

## ARTICLES YOU MAY BE INTERESTED IN

[Giant excitation induced bandgap renormalization in TMDC monolayers](#)

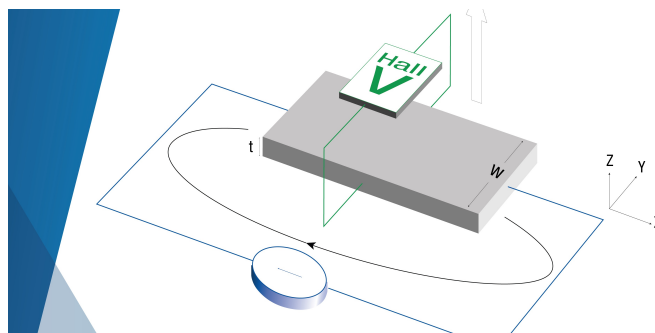
Applied Physics Letters **112**, 061104 (2018); <https://doi.org/10.1063/1.5017069>

[Review Article: Progress in fabrication of transition metal dichalcogenides heterostructure systems](#)

Journal of Vacuum Science & Technology B **35**, 030803 (2017); <https://doi.org/10.1116/1.4982736>

[Band offsets and heterostructures of two-dimensional semiconductors](#)

Applied Physics Letters **102**, 012111 (2013); <https://doi.org/10.1063/1.4774090>



**Tips for minimizing  
Hall measurement errors**

Download the Technical Note



# Observation of inter-layer charge transmission resonance at optically excited graphene–TMDC interfaces

Cite as: APL Mater. 8, 091114 (2020); doi: 10.1063/5.0020396

Submitted: 1 July 2020 • Accepted: 31 August 2020 •

Published Online: 22 September 2020







View Online



Export Citation



CrossMark

Ranjit Kashid,<sup>1</sup>  Jayanta Kumar Mishra,<sup>1</sup> Avradip Pradhan,<sup>1</sup>  Tanweer Ahmed,<sup>1,a)</sup>  Saloni Kakkar,<sup>1</sup> Pranav Mundada,<sup>1</sup> Preeti Deshpande,<sup>2</sup> Kallol Roy,<sup>1</sup> Ambarish Ghosh,<sup>2</sup>  and Arindam Ghosh<sup>1,2,b)</sup>

## AFFILIATIONS

<sup>1</sup>Department of Physics, Indian Institute of Science, Bangalore 560012, India

<sup>2</sup>Centre for Nano Science and Engineering, Indian Institute of Science, Bangalore 560012, India

<sup>a)</sup> Author to whom correspondence should be addressed: [tanweer@iisc.ac.in](mailto:tanweer@iisc.ac.in)

<sup>b)</sup> Electronic mail: [arindam@iisc.ac.in](mailto:arindam@iisc.ac.in)

## ABSTRACT

The transfer of charge carriers across the optically excited hetero-interface of graphene and semiconducting transition metal dichalcogenides (TMDCs) is the key to convert light to electricity, although the intermediate steps from the creation of excitons in TMDC to the collection of free carriers in the graphene layer are not fully understood. Here, we investigate photo-induced charge transport across graphene–MoS<sub>2</sub> and graphene–WSe<sub>2</sub> hetero-interfaces using time-dependent photoresistance relaxation with varying temperature, wavelength, and gate voltage. In both types of heterostructures, we observe an unprecedented resonance in the inter-layer charge transfer rate as the Fermi energy ( $E_F$ ) of the graphene layer is tuned externally with a global back gate. We attribute this to a resonant quantum tunneling from the excitonic state of the TMDC to  $E_F$  of the graphene layer and outline a new method to estimate the excitonic binding energies ( $E_b$ ) in the TMDCs, which are found to be 400 meV and 460 meV in MoS<sub>2</sub> and WSe<sub>2</sub> layers, respectively. The gate tunability of the inter-layer charge transfer timescales may allow precise engineering and readout of the optically excited electronic states at graphene–TMDC interfaces.

© 2020 Author(s). All article content, except where otherwise noted, is licensed under a Creative Commons Attribution (CC BY) license (<http://creativecommons.org/licenses/by/4.0/>). <https://doi.org/10.1063/5.0020396>

The van der Waals (vdW) heterostructures of graphene and transition metal dichalcogenides (TMDCs) are not only outstanding optoelectronic elements<sup>1–22</sup> but also represent atomic scale prototypes of donor–acceptor (DA) complexes,<sup>23–25</sup> where the conversion of photons to free charge carriers can be manipulated with excellent control. In optically excited bulk DA complexes, the excitons dissociate quasi-adiabatically via the transfer of either the electron ( $e$ ) or the hole ( $h$ ) across the interface and form a transient charge transfer state, which directly impacts the quantum efficiency. In the type-II TMDC–TMDC heterostructures, the charge transfer states manifest as inter-layer excitons, resulting in quenching of the intra-layer photoluminescence spectrum.<sup>26–28</sup> In the graphene–TMDC heterostructures, the formation of such inter-layer bound states could not be observed,<sup>19–21</sup> possibly due to strong screening by the graphene layer.<sup>29</sup> The ultra-fast cross-interface selective

transfer of the photo-excited delocalized charge carriers has been demonstrated in graphene–TMDC<sup>19–22</sup> heterostructures, occurring with picosecond timescales. However, significant debate persists regarding the directionality of the charge transfer,<sup>22</sup> as well as the role of Förster type energy transfer<sup>20</sup> across the hetero-interface when the excitons are excited in the TMDC layer. An insight into the exciton dissociation process in the graphene–TMDC heterostructures can be obtained by tuning the Fermi energy ( $E_F$ ) of graphene, which is also expected to affect the rate of charge transfer. However, most ultra-fast pump–probe experiments probing the charge transfer kinetics are limited in the tunability of  $E_F$ , especially those without field-effect transistor (FET) geometry. Here, we have explored the  $e$ – $h$  separation process at graphene–TMDC hetero-interfaces in the FET geometry using time ( $t$ )-dependent photoresistance relaxation. We quantitatively link the

photoresistance relaxation to an inter-layer electron transfer process in which the photo-excited electron undergoes a phonon-assisted transfer from the excitonic state (EX) of the TMDC to the Fermi surface of the graphene layer. The rate ( $\tau_i^{-1}$ ) of this TMDC  $\rightarrow$  graphene electron transfer process is observed to be sharply peaked around a characteristic value of  $E_F$  (measured with respect to the Dirac point of graphene) in both graphene–MoS<sub>2</sub> and graphene–WSe<sub>2</sub> heterostructures. We attribute this to a resonance-like phenomenon when  $E_F$  in graphene aligns with the EX state in the TMDC layer. We also obtain estimations of excitonic binding energies ( $E_b$ )  $\approx$ 400 meV and 460 meV for the monolayers of MoS<sub>2</sub> and WSe<sub>2</sub>, respectively, which closely match with the previous studies.<sup>30–33</sup> Our time-dependent photoresistance measurements may not only be relevant to ultra-fast photodetection and thermalization<sup>34</sup> in graphene–TMDC vdW heterostructures but also form a new and unique spectroscopic tool to probe the optical states in TMDCs.

The graphene–TMDC vdW heterostructures were created using the layer-by-layer transfer of individual mechanically exfoliated graphene and TMDC flakes to form the vertical heterostructures<sup>35,36</sup> [Fig. 1(a)], which were then transferred onto SiO<sub>2</sub>/p<sup>++</sup>-Si substrates, where the heavily doped Si acts as the global backgate. We have performed experiments on one graphene–WSe<sub>2</sub> and two graphene–MoS<sub>2</sub> heterostructures (devices 1 and 2), where single molecular layers of both graphene and TMDC were used. Figure 1(b) shows an optical micrograph of a graphene–MoS<sub>2</sub> heterostructure (device 1) turned FET. The Raman spectra of individual flakes, device fabrication and details, and optical source calibration are shown in Figs. S1–S3 of the supplementary material, respectively. Thermally evaporated Cr/Au contacts on the top surface are used to measure the electrical resistance of the graphene layer. For wavelength dependent optical illumination, we used a tungsten–halogen lamp (Horiba, LSH-T250), which acts as a continuous optical source over the wavelength ( $\lambda$ ) of interest ( $\approx$ 550 nm–800 nm).

The band alignment at the graphene–TMDC interface, which is similar for both graphene–MoS<sub>2</sub><sup>9</sup> and graphene–WSe<sub>2</sub><sup>37</sup> heterostructures, suggests energy offset of  $\approx$ 0.30 eV and  $\approx$ 0.50 eV, respectively, between the Dirac point of graphene and the minimum ( $E_C$ ) of the quasi-particle conduction band of the TMDC layer [in Fig. 1(c)]. The photoluminescence (PL) spectra from our devices were obtained using a HORIBA LabRam HR tool under high vacuum condition (pressure  $\sim 10^{-5}$  mbar). The PL from the TMDC layer underneath graphene is quenched compared to that from the bare TMDC region [Fig. 1(d) for the graphene–WSe<sub>2</sub> heterostructure], confirming the significant decay of TMDC's excitons in nonradiative pathways such as TMDC  $\rightarrow$  graphene electron transfer.<sup>2,5,8,12,20,22</sup> While the stronger quenching at room temperature than at 40 K can indicate a competition between TMDC  $\rightarrow$  graphene electron transfer timescale ( $\tau_i$ ) and radiative lifetimes ( $\tau_r$ ),<sup>38,39</sup> the PL quenching may also be due to the Förster-type energy transfer across the vdW interface in the graphene–TMDC heterostructures<sup>20</sup> (see Fig. S4 of the supplementary material for PL quenching in the graphene–MoS<sub>2</sub> heterostructure). The direct evidence of the charge transfer was established earlier when such heterostructures were implemented in the FET architecture.<sup>1,4,18</sup>

The transfer of charge following the dissociation of the excitons changes the resistance ( $R$ ) of the graphene layer. Figure 2(a) illustrates the  $R$  vs back gate voltage ( $V_G$ ) characteristic of a graphene–WSe<sub>2</sub> heterostructure, which is close to that of the pristine graphene because the WSe<sub>2</sub> layer itself is highly resistive ( $>M\Omega$ ) [see Fig. S5(a) of the supplementary material for the graphene–MoS<sub>2</sub> heterostructure]. When the optical illumination is turned on,  $R$  decreases (increases) from  $R_{off}$  to  $R_{on}$  in the electron (hole)-doped regime, indicating the transfer of electrons from the TMDC layer to graphene [Fig. 2(b) and Fig. S5(b) of the supplementary material for the graphene–MoS<sub>2</sub> heterostructure]. Here,  $R_{off}$  and  $R_{on}$  are the steady state resistances of the graphene layer without and with the optical illumination, respectively. This observation is consistent with

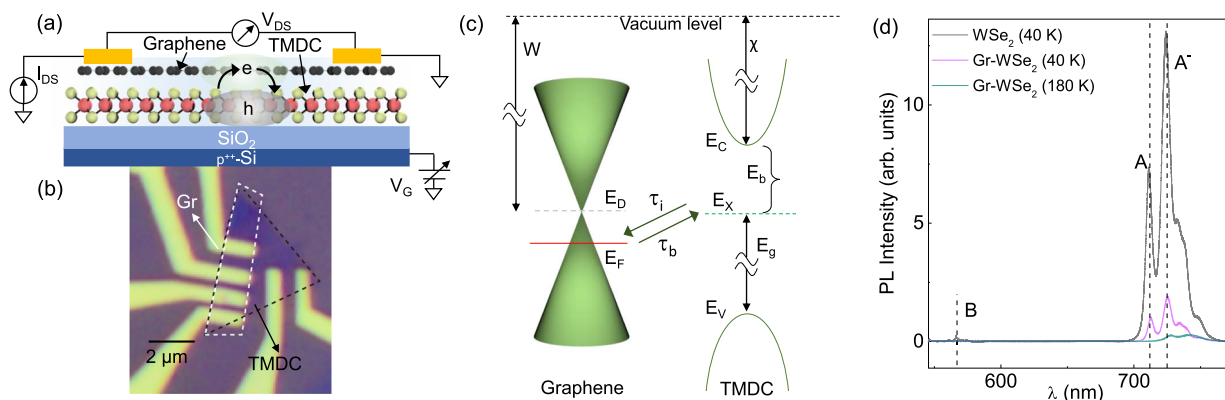


**FIG. 1.** (a) Schematic of the graphene–TMDC heterostructure along with the circuit diagram for opto-electronic measurement. (b) Optical micrograph of a typical graphene–TMDC heterostructure device. (c) Relative band alignment showing the relevant energy scales for generic graphene–TMDC heterostructures. Here,  $W$ ,  $\chi$ ,  $E_D$ ,  $E_F$ ,  $E_x$ ,  $E_g$ , and  $E_b$  are the work function of undoped graphene, electron affinity of the TMDC layer, energy at the Dirac point, Fermi energy of graphene, excitonic energy level inside the TMDC layer, optical band gap of TMDC, and the binding energy of the excitons, respectively.  $\tau_i$  and  $\tau_b$  are the timescales of photogenerated electron transfer in the TMDC  $\rightarrow$  graphene and graphene  $\rightarrow$  TMDC directions, respectively. (d) Photoluminescence (PL) spectra of graphene–WSe<sub>2</sub> heterostructures showing the quenching of the PL signal in the heterostructure region in comparison to bare WSe<sub>2</sub>. A, B, and A<sup>-</sup> indicate the excitonic and negatively charged trionic transitions, respectively.

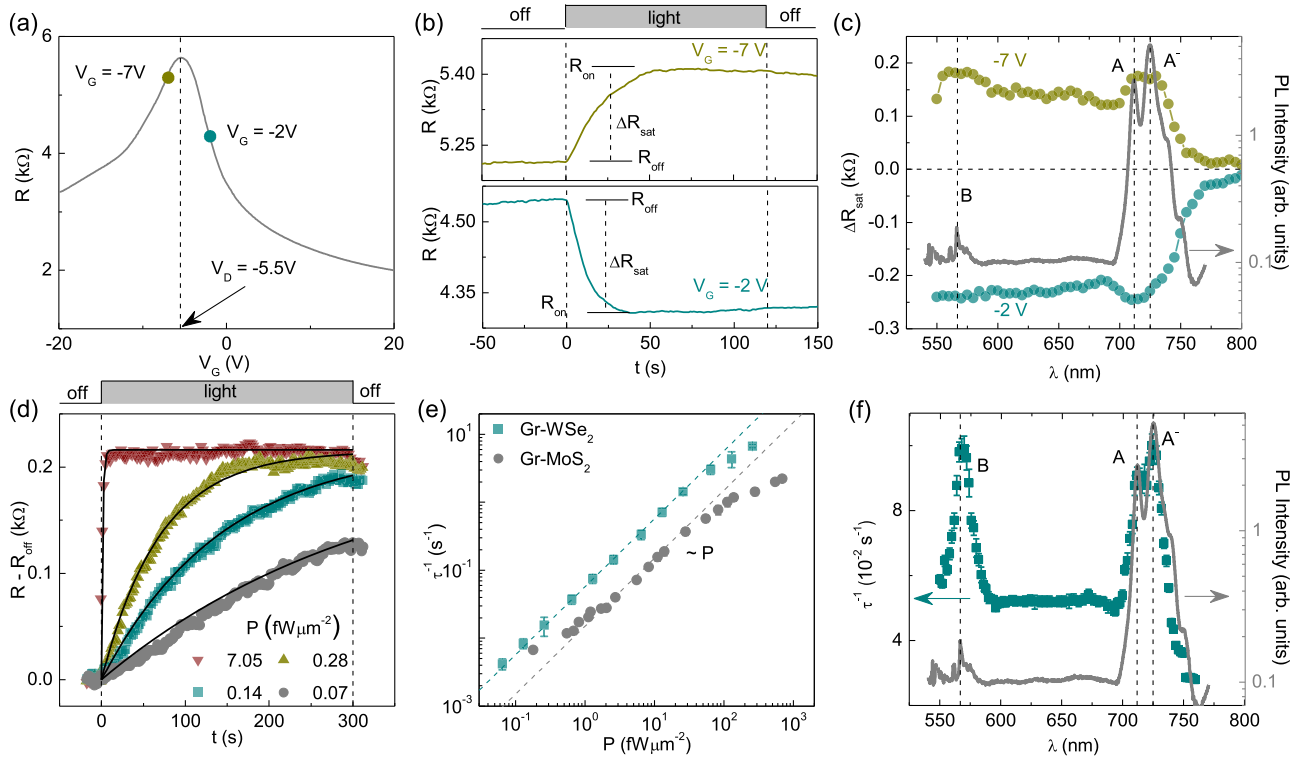


**FIG. 2.** (a) Resistance ( $R$ )–gate voltage ( $V_G$ ) characteristics of a graphene–WSe<sub>2</sub> heterostructure shown in Fig. 1(b). (b) Change in  $R$  for a 120 s optical pulse at illumination power  $P = 0.56 \text{ fW } \mu\text{m}^{-2}$  and wavelength  $\lambda = 600 \text{ nm}$ . The increase and decrease in  $R$  are observed for the hole-doped ( $V_G = -7 \text{ V}$ ) and electron-doped ( $V_G = -2 \text{ V}$ ) regimes, respectively. (c)  $\Delta R_{\text{sat}}$  as a function of  $\lambda$  showing the suppression of photoresponse for photon energy  $E_\lambda > E_g$  (for monolayer WSe<sub>2</sub>,  $E_g \approx 1.74 \text{ eV}$ ). (d) Exponential relaxation of  $R$  for the different power level ( $P$ ) of optical excitation (at  $\lambda = 600 \text{ nm}$ ). The black lines are fits to the data. (e) Dependence of the relaxation rate ( $\tau^{-1}$ ) on the excitation power ( $P$ ) for both graphene–MoS<sub>2</sub> and graphene–WSe<sub>2</sub> heterostructures. The experiments are performed in vacuum at  $T = 85 \text{ K}$ , except for PL in (c) and (f) performed at  $T = 40 \text{ K}$ .

the earlier reports on the photoresistance in the graphene–TMDC heterostructures<sup>1,4</sup> and can also be viewed as a photogating effect, where the net photoresistance  $\Delta R_{\text{sat}} = dR/dV_G \times eN_g/C_{\text{ox}}$  is the result of an effective change in  $V_G$ . Here,  $N_g$  is the total change in the carrier density in the graphene channel by virtue of TMDC  $\rightarrow$  graphene electron transfer once the system reaches the steady state,  $C_{\text{ox}}$  is the capacitance of the 290 nm SiO<sub>2</sub> per unit area, and  $e$  is the electronic charge. This is further confirmed by the observed proportionality of  $\Delta R_{\text{sat}}$  and  $dR/dV_G$  (see Fig. S6 of the supplementary material). Here,  $\Delta R_{\text{sat}}$  is persistent, and the transferred electron (in graphene) and hole (in TMDC) do not recombine even after the illumination is turned off, unless a positive pulse of  $\geq 20 \text{ V}$  in  $V_G$  is applied to reset the device.<sup>1</sup> The persistence indicates a strongly suppressed electron backflow to the TMDC layer due to the paucity of available states in TMDC at the Fermi level of graphene. Importantly,  $\Delta R_{\text{sat}}$  [see Fig. 2(c)] is nonzero only for the photon energies ( $E_\lambda = hc/\lambda$ , where  $h$  and  $c$  are the Planck constant and velocity of light, respectively) at which the optical density-of-states (DoS) in the TMDC layer is nonzero, as confirmed from the comparison of the PL and  $\Delta R_{\text{sat}}$  [Fig. 2(c), also shown in Fig. S5(c) of the supplementary material for data from the graphene–MoS<sub>2</sub> device]. The wavelength dependent photoresistance measurements were performed at  $T = 85 \text{ K}$ , with an

illumination power density ( $P$ ) of  $0.56 \text{ fW } \mu\text{m}^{-2}$ . The absence of the photoresponse at  $E_\lambda < \text{optical bandgap } (E_g)$  of the WSe<sub>2</sub> allows us to ignore the photo-thermionic charge transfer in our devices.<sup>13,22</sup>

Figure 2(d) presents the time-dependent photoresistance relaxation data at different power densities ( $P$ ) of the incident illumination with  $\lambda = 600 \text{ nm}$  from the graphene–WSe<sub>2</sub> device at  $V_G = -7 \text{ V}$  and  $T = 85 \text{ K}$  (see Fig. S5 of the supplementary material for the data from the graphene–MoS<sub>2</sub> device). In this case, the power calibrated LED was used as the source of optical illumination.  $R(t) = R_{\text{off}} + \Delta R_{\text{sat}} \times (1 - \exp(-t/\tau))$  [solid lines in Fig. 2(d)] behavior is observed at all values of  $P$ , where  $\tau$  is the timescale of the photoresponse.  $\tau$  is observed to be inversely proportional to  $P$  over the experimental range of  $P$ .  $\tau^{-1} \propto P$  behavior from both graphene–MoS<sub>2</sub> and graphene–WSe<sub>2</sub> devices is presented in Fig. 2(e). The dashed lines indicate linear fits to the data.

The exponential relaxation can be understood in terms of charge in-flow and out-flow rates to/from graphene. Following the generation of the exciton with the radiative lifetime  $\tau_r$  in TMDC, the electron makes transition to graphene with the inter-layer charge transfer timescale  $\tau_i$ . This leads to a negative (positive)  $\Delta R$  in graphene in the electron (hole) doped regime. The  $P$  independent  $\Delta R_{\text{sat}}$  [Fig. 2(d)] indicates a  $P$  independent number density ( $N_g$ )

of electron transfer. Considering the electron transfer rate  $(N_g - n_g)/(N_g\tau_i)$  from the EX state (having energy  $E_X$ ) to graphene, the electron transfer dynamics under the optical illumination can be expressed as<sup>18</sup>

$$\frac{dn_g}{dt} = \frac{n_e(N_g - n_g)}{N_g\tau_i} - \frac{n_g}{\tau_b} \quad (1)$$

Here,  $n_g$  is the transferred electron density at time  $t$  and  $n_e = \phi_a\tau_r$  is the photo-excited electron density in the TMDC. The  $\phi_a = \alpha_\lambda P/E_\lambda$  is the absorbed photon flux, where  $\alpha_\lambda$  is the absorption coefficient of the monolayer TMDC. Considering electron's back transfer (graphene  $\rightarrow$  TMDC) timescale  $\tau_b \gg \tau_i$  at  $E_F \ll E_X$ , we obtain the solution of Eq. (1) as  $n_g(t) = N_g \times (1 - \exp(-t/\tau))$ . This leads to a time-dependent photoresistance relaxation, where  $\tau = (\tau_i/\tau_r)(N_g/\phi_a)$  is the timescale of photoresistance relaxation (see Fig. S7 of the supplementary material for the  $\tau$  calculation details). This agrees well with the observed  $\tau^{-1} \propto P$  ( $\tau^{-1} \propto \phi_a$ ) behavior. Intriguingly,  $\tau^{-1} (\propto \alpha_\lambda)$  follows closely the optical DoS of the TMDC underlayer [Fig. 2(f) (WSe<sub>2</sub>) and Fig. S5e of the supplementary material (MoS<sub>2</sub>)]. The  $\alpha_\lambda$  demonstrates maxima at the excitonic and trionic ( $A, A^-$ , and  $B$ ) energies in TMDCs, leading to the

maxima in  $\tau^{-1}$  at those energies. The wavelength dependent  $\tau^{-1}$  measurements were performed at  $T = 85$  K, with an illumination power density ( $P$ ) of  $0.56 \text{ fW } \mu\text{m}^{-2}$ . Considering a typical value of  $\tau_r = 1 \text{ ps}$ <sup>38,40</sup> at low  $T, N_g \sim 10^{11} \text{ cm}^{-2}$  (see Fig. S8 of the supplementary material), and  $\alpha_\lambda = 10\%$  in the monolayer TMDC,<sup>41</sup> and using the observed  $\tau^{-1} \propto P$  relation [Fig. 2(e)], we estimate  $\tau_i \approx 4 \text{ ps}$  in the graphene-WSe<sub>2</sub> heterostructure at 80 K. This matches well with the charge transfer timescales observed using the pump-probe experiments.<sup>12,20,22</sup> Although charge trapping can play an important role in the photoresponse of bare TMDC phototransistors<sup>42</sup> (see Fig. S10 of the supplementary material), ultrafast TMDC  $\rightarrow$  graphene charge transfer, facilitated by  $\tau_i \approx 4 \text{ ps}$ , constitutes the primary source of photoresponse in our graphene-TMDC devices.

The quantitative relation between the photoresistance relaxation rate  $\tau^{-1}$  and the charge transfer rate  $\tau_i^{-1}$  allows us to monitor the charge transfer process as a function of energy difference between graphene's  $E_F$  and the EX state of the TMDC layer. We have performed the  $V_G$  dependent photoresistance relaxation experiments in both graphene-WSe<sub>2</sub> and graphene-MoS<sub>2</sub> devices. Converting the instantaneous photoresistance  $[\Delta R(t)]$  to  $n_g$  using  $n_g = \Delta RC_{ox}/(edR/dV_G)$ , we plot the normalized  $n_g(t)$  in Fig. 3(a) at

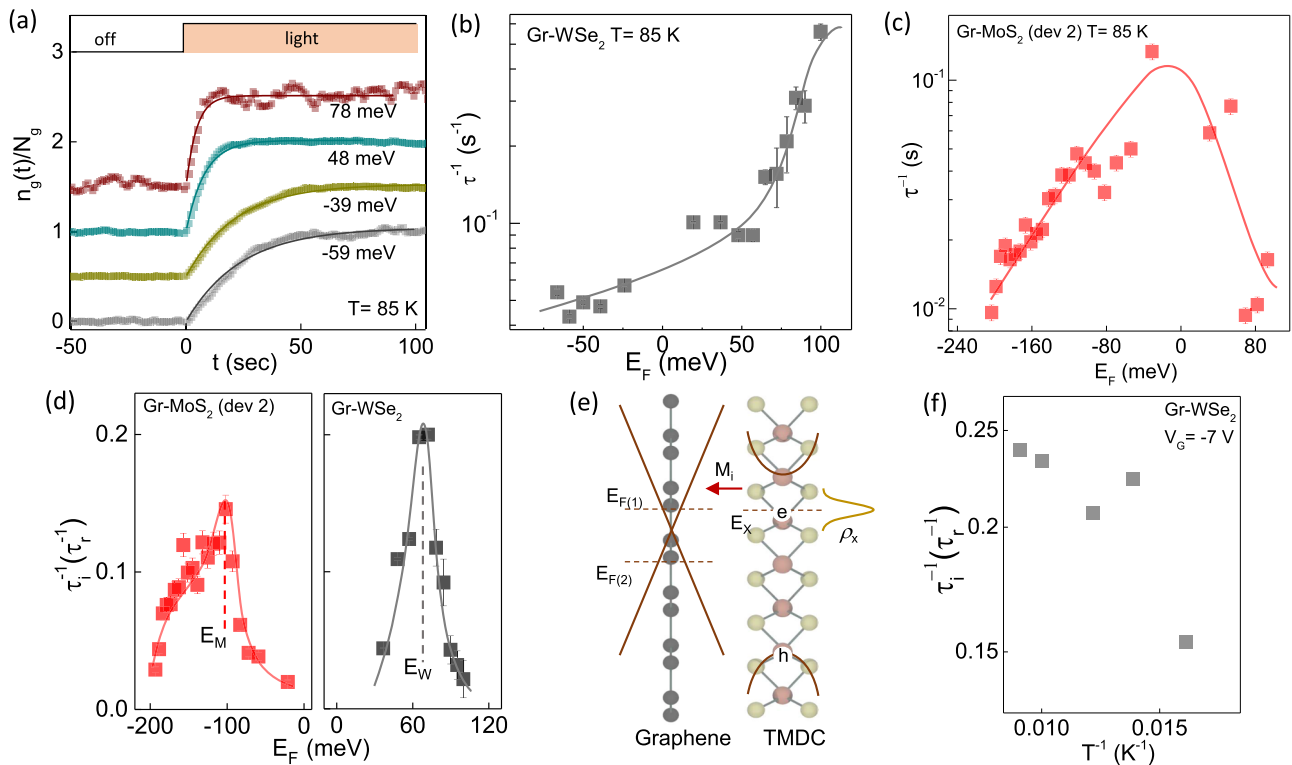


**FIG. 3.** (a)  $n_g/N_g$  vs time data from the graphene-WSe<sub>2</sub> heterostructure during the light off-on cycle with  $P = 0.56 \text{ fW } \mu\text{m}^{-2}$ . The data at different  $E_F$  values are shifted vertically for clarity. The solid lines present exponential fits. [(b) and (c)]  $\tau^{-1}$  (at  $P = 0.56 \text{ fW } \mu\text{m}^{-2}$  using  $\lambda = 600 \text{ nm}$ ) from graphene-WSe<sub>2</sub> and graphene-MoS<sub>2</sub> heterostructures, respectively, are plotted as a function of the  $E_F$ . (d) Extracted  $\tau_i^{-1}$  vs  $E_F$  data (in units of  $\tau_r^{-1}$ ) from the graphene-WSe<sub>2</sub> (right panel) and graphene-MoS<sub>2</sub> (left panel) heterostructures. The solid lines in Figs. 3(b)–3(d) are guides to the eye. (e) The resonance in  $\tau_i^{-1}$  is schematically presented. The energy band diagrams of graphene and TMDC are schematically shown. The DoS of the EX ( $\rho_x$ ) state is marked in orange trace.  $E_F$  values at different  $V_G$  values are shown using dashed lines. (f)  $\tau_i^{-1}$  vs  $T^{-1}$  data are presented.

different values of  $E_F$  [=  $\pm \hbar v_F \sqrt{C_{ox}}(V_G - V_D)/e$ , where  $\hbar$ ,  $V_D$ , and  $v_F$  are the reduced Planck constant, gate voltage at the charge neutrality point, and the Fermi velocity in graphene, respectively; the “+” and “-” signs are for  $V_G > V_D$  and  $V_G < V_D$ , respectively] from the graphene-WSe<sub>2</sub> heterostructure at  $P = 0.56 \text{ fW } \mu\text{m}^{-2}$  and  $\lambda = 600 \text{ nm}$  (shifted vertically for clarity). The characteristic  $\tau$  is clearly dependent on  $E_F$ . To confirm this, we calculated  $\tau^{-1}$  from the exponential fit and plotted it as a function of  $E_F$  in Figs. 3(b) and 3(c) for graphene-WSe<sub>2</sub> and graphene-MoS<sub>2</sub> devices, respectively. The solid traces are guides to the eye. Using the experimentally observed  $\tau$  and  $N_g$  (see Fig. S8 of the supplementary material for  $N_g$  vs  $E_F$  data from both devices), we then calculate the TMDC  $\rightarrow$  graphene electron transfer rate  $\tau_i^{-1} = \tau_r^{-1} \tau^{-1} N_g / \phi_a$ , which exhibits a sharply peaked [Figure 3(d), the solid traces are guides to the eye] variation with  $E_F$ , with the peak positions around  $E_F \approx -100 \text{ meV}$  ( $E_M$ ) and  $E_F \approx 70 \text{ meV}$  ( $E_W$ ) in graphene-MoS<sub>2</sub> and graphene-WSe<sub>2</sub> devices, respectively. Notably, the FWHM (full width at half maxima)  $\sim 100 \text{ meV}$  to  $50 \text{ meV}$  of the peaks closely corresponds to the excitonic linewidth of TMDC observed in the PL spectra [Fig. 1(d) and Fig. S5 of the supplementary material]. This suggests a possible resonance of  $E_F$  with the EX state in WSe<sub>2</sub> (MoS<sub>2</sub>) at  $E_F = E_{W(M)}$ . To verify this, we calculate the excitonic binding energy in WSe<sub>2</sub> (MoS<sub>2</sub>),  $E_b = W - E_{W(M)} - \chi_{W(M)}$ , considering the undoped graphene’s work function  $W \approx 4.56 \text{ eV}^{43}$  and the electron affinity of WSe<sub>2</sub> (MoS<sub>2</sub>),  $\chi_{W(M)} \approx 4.06 \text{ eV}^{37}$  ( $4.27 \text{ eV}^{44}$ ). In the literature, the reported values of  $W$  and  $\chi_{W(M)}$  show approximately few tens of meV variations [see Fig. S9(a) of the supplementary material for a detailed review], resulting in up to  $\sim 50 \text{ meV}$  difference between the actual  $E_b$  and its calculated value. The  $E_b$  of monolayer WSe<sub>2</sub> and MoS<sub>2</sub> were previously studied both experimentally and theoretically. The reported values show significant variations falling within the range of  $\sim 300 \text{ meV}$ – $700 \text{ meV}$  (see Fig. S9 of the supplementary material for a detailed review). Our estimated  $E_b \approx 460 \text{ meV}$  and  $400 \text{ meV}$  for WSe<sub>2</sub> and MoS<sub>2</sub>, respectively, match closely with the experimentally reported  $E_b$  using PL,<sup>30,31</sup> transient absorption,<sup>32</sup> and photoresistance spectroscopy<sup>33</sup> and also with the theoretical results using various approaches of the effective mass model.<sup>45–49</sup>

Resonant electron transfer is commonly observed in the tunneling diodes and the tunneling spectroscopy studies,<sup>50</sup> which generally occurs via the phonon or the defect-assisted pathways.<sup>51</sup> Here, the electron transfer mechanism is schematically described in Fig. 3(e). The  $E_F$  of graphene is indicated at and away from the resonance ( $E_{F(1)}$  and  $E_{F(2)}$ , respectively). The DoS of the EX state is indicated as  $\rho_X$ .  $M_i(E_X, E_F)$  is the TMDC  $\rightarrow$  graphene transmission matrix element containing the wavefunction overlap integral. The charge transfer rate  $\tau_i^{-1}$  is proportional to  $|M_i|^2$ . At  $E_X = E_F$ , the resonance causes large  $|M_i|^2$ , which gives rise to the peaked behavior in  $\tau_i^{-1}$ . Figure 3(f) presents the  $\tau_i^{-1}$  vs  $T^{-1}$  data from the graphene-WSe<sub>2</sub> heterostructure at  $V_G = -7 \text{ V}$ .  $\tau_i^{-1}$  increases with an increase in  $T$ , with an activation energy  $\approx 7 \text{ meV}$ , indicating a phonon-assisted electron transfer process, which is previously reported to occur across TMDC interfaces.<sup>52–55</sup> In our heterostructures,  $\tau_i^{-1} < \tau_r^{-1}$  behavior is observed, which can be related to the inter-layer coupling between graphene and TMDC layers.  $\tau_i^{-1} \gg \tau_r^{-1}$  behavior is previously reported in graphene-TMDC heterostructures, which requires an exceptionally coupled interface, where the separation ( $d$ ) between the monolayers of graphene and TMDC is  $\approx 3 \text{ \AA}$ – $6 \text{ \AA}$ ,<sup>20,22</sup> leading

to a large PL quenching (by factor of  $\sim 250$ ) in the overlap region.<sup>20</sup> With an increase in  $d$ ,  $|M_i|^2$  reduces and  $\tau_i$  increases, which degrades the PL quenching effect,<sup>20,22,56</sup> which is consistent with the weaker PL quenching in our heterostructures {up to factor of 5 and 1.5 in the graphene-WSe<sub>2</sub> [Fig. 1(d)] and graphene-MoS<sub>2</sub> (Fig. S4 of the supplementary material) heterostructure, respectively}.

Apart from the charge transfer rate, the magnitude of the charge transfer is also affected when  $E_F$  is dynamically tuned with respect to the EX state. Here, we observe that  $N_g$  decreases rapidly when  $E_F$  approaches increasingly closer to the EX state.  $N_g$  vs  $E_F - E_X$  data [Fig. 4(a)] from the graphene-WSe<sub>2</sub>(MoS<sub>2</sub>) heterostructure at  $T = 85 \text{ K}$  ( $180 \text{ K}$ ) show  $N_g \propto \exp(-\frac{E_F - E_X}{k_B T})$  behavior (solid lines), confirming that the loss of  $N_g$  occurs via a thermally activated process. Such thermally activated graphene  $\rightarrow$  MoS<sub>2</sub> transfer of electrons has been discussed previously<sup>22</sup> and represented by the  $-n_g/\tau_b$  term in Eq. (1), that cannot be ruled out in the  $|E_X - E_F| \sim k_B T$  regime. At equilibrium (after  $R_{on}$  is reached),  $E_X$  and  $E_F$  can act as a two state system, where  $n_e/\tau_i = N_g/\tau_b$  or  $N_g \propto \tau_b$  condition should be satisfied ( $n_e$  is the number density of electrons in EX). The rate of the thermal activation of the electrons from the  $E_F$  to the EX state is  $\tau_b^{-1} \propto \exp(-\frac{\Delta_B}{k_B T})$ , where  $\Delta_B \approx E_X - E_F$ , which

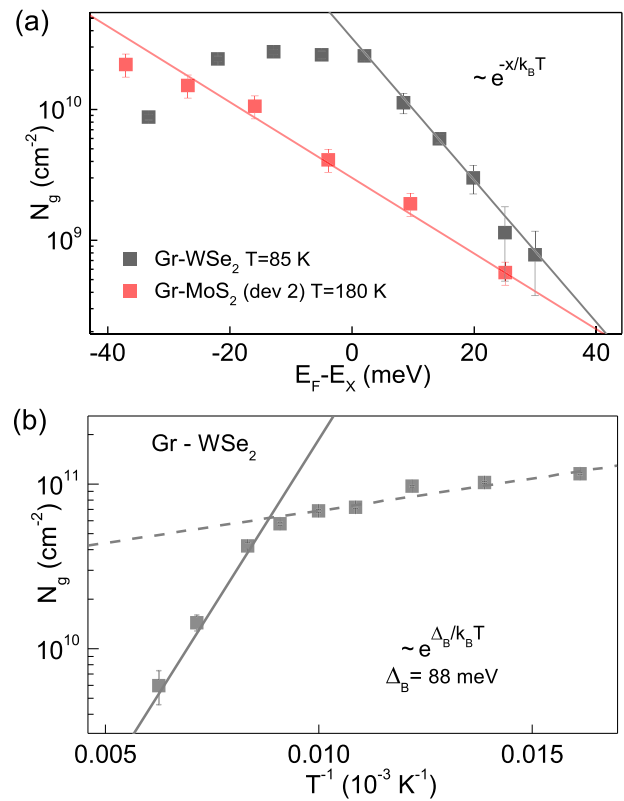


**FIG. 4.** (a)  $N_g$  (recorded at  $P \approx 0.56 \text{ fW } \mu\text{m}^{-2}$ ), from the graphene-WSe<sub>2</sub> (at  $T = 85 \text{ K}$ ) and graphene-MoS<sub>2</sub> (at  $T = 180 \text{ K}$ ) heterostructures, is plotted as a function of  $E_F - E_X$ . The solid lines present the  $N_g \propto \exp(-\frac{E_F - E_X}{k_B T})$  fit. (b) Temperature-dependence of  $N_g$ . The black solid and dashed lines correspond to activation energies  $\approx 88 \text{ meV}$  and  $8 \text{ meV}$ , respectively.

gives rise to the activated behavior of  $N_g$  observed in Fig. 4(a). This is further verified by the  $T$  dependence of  $N_g$  [Fig. 4(b)] at  $E_F - E_X \approx -100$  meV ( $V_G = -7$  V). In a sufficiently high  $T$  range ( $T > 100$  K),  $N_g$  decreases with an activation energy  $\Delta_B \approx 88$  meV (solid black line) that closely matches with the corresponding  $E_X - E_F$  and validates a thermally activated scenario of electron's back transfer from  $E_F$  to the EX state. At  $T \leq 100$  K, a much lower activation energy of  $\approx 8$  meV is observed, which closely matches with the phonon energies in monolayer WSe<sub>2</sub>, indicating a phonon-assisted pathway of electron transfer from  $E_F$  to the EX state. Figures 3(f) and 4(b) suggest that the phonons<sup>52–55</sup> can play a crucial role in graphene  $\leftrightarrow$  TMDC inter-layer charge exchange in our heterostructures in the low temperature range ( $T \leq 100$  K).

In summary, using the time-dependent relaxation of photoresistance in the field-effect architecture, we have identified a new resonant electron transfer from the excitonic (EX) state of TMDC to the Fermi energy ( $E_F$ ) of graphene and a thermally activated back transfer electron from  $E_F$  to the EX state in optically excited graphene–MoS<sub>2</sub> and graphene–WSe<sub>2</sub> heterostructures. Our experiments yield a reasonable estimation of the excitonic binding energies ( $E_b$ ) in both MoS<sub>2</sub> and WSe<sub>2</sub>. We have demonstrated precise controllability on timescales and magnitudes of charge transfer by tuning the temperature and gate voltage.

See the [supplementary material](#) for Raman spectroscopy on individual flakes, device fabrication and details, optical source calibration, photoluminescence (PL) spectra of the graphene–MoS<sub>2</sub> heterostructure, photocurrent measurement of the graphene–MoS<sub>2</sub> (device 1) hybrid device, photogating effect in graphene–WSe<sub>2</sub> hybrid devices, procedure of transfer rate ( $\tau^{-1}$ ) calculation,  $N_g$  vs  $E_F$  in graphene–TMDC devices, estimation of exciton binding energy ( $E_b$ ), and comparison of photoresponse in the graphene–MoS<sub>2</sub> hybrid and the bare MoS<sub>2</sub> underlayer.

## AUTHORS' CONTRIBUTIONS

R.K., J.K.M., A.P., and T.A. contributed equally to this work.

R.K. acknowledges financial support from Dr. D. S. Kothari postdoctoral fellowship (UGC-DSKPDF), a program by the University Grant Commission (UGC), India. The authors thank NNFC, IISc Bangalore, India, and MNCF, IISc, Bangalore, India, for providing cleanroom fabrication and characterization facilities. The authors also acknowledge DST, Government of India, for funding the project.

## DATA AVAILABILITY

The data that support the findings of this study are available from the corresponding author upon reasonable request.

## REFERENCES

- 1 K. Roy, M. Padmanabhan, S. Goswami, T. P. Sai, G. Ramalingam, S. Raghavan, and A. Ghosh, *Nat. Nanotechnol.* **8**, 826 (2013).
- 2 L. Britnell, R. M. Ribeiro, A. Eckmann, R. Jalil, B. D. Belle, A. Mishchenko, Y. J. Kim, R. V. Gorbachev, T. Georgiou, S. V. Morozov, A. N. Grigorenko, A. K. Geim, C. Casiraghi, A. H. C. Neto, and K. S. Novoselov, *Science* **340**, 1311–1314 (2013).
- 3 S. Ghatak, A. N. Pal, and A. Ghosh, *ACS Nano* **5**, 7707–7712 (2011).
- 4 K. Roy, T. Ahmed, H. Dubey, T. P. Sai, R. Kashid, S. Maliakal, K. Hsieh, S. Shamim, and A. Ghosh, *Adv. Mater.* **30**, 1704412 (2018).
- 5 Y. Li, C.-Y. Xu, J.-K. Qin, W. Feng, J.-Y. Wang, S. Zhang, L.-P. Ma, J. Cao, P. A. Hu, W. Ren, and L. Zhen, *Adv. Funct. Mater.* **26**, 293–302 (2016).
- 6 A. Pradhan, A. Roy, S. Tripathi, A. Som, D. Sarkar, J. K. Mishra, K. Roy, T. Pradeep, N. Ravishankar, and A. Ghosh, *Nanoscale* **9**, 9284–9290 (2017).
- 7 S. Islam, J. K. Mishra, A. Kumar, D. Chatterjee, N. Ravishankar, and A. Ghosh, *Nanoscale* **11**, 1579–1586 (2019).
- 8 Y. Li, J.-K. Qin, C.-Y. Xu, J. Cao, Z.-Y. Sun, L.-P. Ma, P. A. Hu, W. Ren, and L. Zhen, *Adv. Funct. Mater.* **26**, 4319–4328 (2016).
- 9 S. Larentis, J. R. Tolsma, B. Fallahzad, D. C. Dillen, K. Kim, A. H. MacDonald, and E. Tutuc, *Nano Lett.* **14**, 2039–2045 (2014).
- 10 D. Pierucci, H. Henck, J. Avila, A. Balan, C. H. Naylor, G. Patriarche, Y. J. Dappe, M. G. Silly, F. Sirotti, A. T. C. Johnson, M. C. Asensio, and A. Ouerghi, *Nano Lett.* **16**, 4054–4061 (2016).
- 11 H. Coy Diaz, J. Avila, C. Chen, R. Addou, M. C. Asensio, and M. Batzill, *Nano Lett.* **15**, 1135–1140 (2015).
- 12 M. Massicotte, P. Schmidt, F. Vialla, K. G. Schädler, A. Reserbat-Plantey, K. Watanabe, T. Taniguchi, K. J. Tielrooij, and F. H. L. Koppens, *Nat. Nanotechnol.* **11**, 42 (2016).
- 13 M. Massicotte, P. Schmidt, F. Vialla, K. Watanabe, T. Taniguchi, K.-J. Tielrooij, and F. H. Koppens, *Nat. Commun.* **7**, 12174 (2016).
- 14 J. Y. Tan, A. Avsar, J. Balakrishnan, G. K. W. Koon, T. Taychatanapat, E. C. T. O'Farrell, K. Watanabe, T. Taniguchi, G. Eda, A. H. Castro Neto, and B. Özyilmaz, *Appl. Phys. Lett.* **104**, 183504 (2014).
- 15 M. Ghorbani-Asl, P. D. Bristowe, K. Koziol, T. Heine, and A. Kuc, *2D Mater.* **3**, 025018 (2016).
- 16 C. E. Giusca, I. Rungger, V. Panchal, C. Melios, Z. Lin, Y.-C. Lin, E. Kahn, A. L. Elias, J. A. Robinson, M. Terrones, and O. Kazakova, *ACS Nano* **10**, 7840–7846 (2016).
- 17 W. Zhang, C.-P. Chuu, J.-K. Huang, C.-H. Chen, M.-L. Tsai, Y.-H. Chang, C.-T. Liang, Y.-Z. Chen, Y.-L. Chueh, J.-H. He, M.-Y. Chou, and L.-J. Li, *Sci. Rep.* **4**, 3826 (2014).
- 18 T. Ahmed, K. Roy, S. Kakkar, A. Pradhan, and A. Ghosh, *2D Mater.* **7**, 025043 (2020).
- 19 C. Lu, C. Quan, K. Si, X. Xu, C. He, Q. Zhao, Y. Zhan, and X. Xu, *Appl. Surf. Sci.* **479**, 1161–1168 (2019).
- 20 G. Froehlicher, E. Lorchat, and S. Berciaud, *Phys. Rev. X* **8**, 011007 (2018).
- 21 J. He, N. Kumar, M. Z. Bellus, H.-Y. Chiu, D. He, Y. Wang, and H. Zhao, *Nat. Commun.* **5**, 5622 (2014).
- 22 L. Yuan, T.-F. Chung, A. Kuc, Y. Wan, Y. Xu, Y. P. Chen, T. Heine, and L. Huang, *Sci. Adv.* **4**, e1700324 (2018).
- 23 A. A. Bakulin, A. Rao, V. G. Pavelyev, P. H. M. van Loosdrecht, M. S. Pshenichnikov, D. Niedzialek, J. Cornil, D. Beljonne, and R. H. Friend, *Science* **335**, 1340–1344 (2012).
- 24 A. E. Jaiilaubekov, A. P. Willard, J. R. Tritsch, W.-L. Chan, N. Sai, R. Gearba, L. G. Kaake, K. J. Williams, K. Leung, P. J. Rossky, and X.-Y. Zhu, *Nat. Mater.* **12**, 66 (2013).
- 25 H. Tamura and I. Burghardt, *J. Am. Chem. Soc.* **135**, 16364–16367 (2013).
- 26 X. Hong, J. Kim, S.-F. Shi, Y. Zhang, C. Jin, Y. Sun, S. Tongay, J. Wu, Y. Zhang, and F. Wang, *Nat. Nanotechnol.* **9**, 682 (2014).
- 27 F. Ceballos, M. Z. Bellus, H.-Y. Chiu, and H. Zhao, *ACS Nano* **8**, 12717–12724 (2014).
- 28 X. Zhu, N. R. Monahan, Z. Gong, H. Zhu, K. W. Williams, and C. A. Nelson, *J. Am. Chem. Soc.* **137**, 8313–8320 (2015).
- 29 A. Raja, A. Chaves, J. Yu, G. Arefe, H. M. Hill, A. F. Rigosi, T. C. Berkelbach, P. Nagler, C. Schüller, T. Korn, C. Nuckolls, J. Hone, L. E. Brus, T. F. Heinz, D. R. Reichman, and A. Chernikov, *Nat. Commun.* **8**, 15251 (2017).
- 30 K. He, N. Kumar, L. Zhao, Z. Wang, K. F. Mak, H. Zhao, and J. Shan, *Phys. Rev. Lett.* **113**, 026803 (2014).
- 31 H. M. Hill, A. F. Rigosi, C. Roquelet, A. Chernikov, T. C. Berkelbach, D. R. Reichman, M. S. Hybertsen, L. E. Brus, and T. F. Heinz, *Nano Lett.* **15**, 2992–2997 (2015).

- <sup>32</sup>L. Wang, Z. Wang, H.-Y. Wang, G. Grinblat, Y.-L. Huang, D. Wang, X.-H. Ye, X.-B. Li, Q. Bao, A.-S. Wee, S. A. Maier, Q.-D. Chen, M.-L. Zhong, C.-W. Qiu, and H.-B. Sun, *Nat. Commun.* **8**, 13906 (2017).
- <sup>33</sup>A. Klots, A. Newaz, B. Wang, D. Prasai, H. Krzyzanowska, J. Lin, D. Caudel, N. Ghimire, J. Yan, B. Ivanov, K. Velizhanin, A. Burger, D. Mandrus, N. Tolc, S. Pantelides, and K. Bolotin, *Sci. Rep.* **4**, 6608 (2014).
- <sup>34</sup>Q. Ma, T. I. Andersen, N. L. Nair, N. M. Gabor, M. Massicotte, C. H. Lui, A. F. Young, W. Fang, K. Watanabe, T. Taniguchi, J. Kong, N. Gedik, F. H. L. Koppens, and P. Jarillo-Herrero, *Nat. Phys.* **12**, 455 (2016).
- <sup>35</sup>C. R. Dean, A. F. Young, I. Meric, C. Lee, L. Wang, S. Sorgenfrei, K. Watanabe, T. Taniguchi, P. Kim, K. L. Shepard, and J. Hone, *Nat. Nanotechnol.* **5**, 722 (2010).
- <sup>36</sup>P. J. Zomer, S. P. Dash, N. Tombros, and B. J. Van Wees, *Appl. Phys. Lett.* **99**, 232104 (2011).
- <sup>37</sup>K. Kim, S. Larentis, B. Fallahzad, K. Lee, J. Xue, D. C. Dillen, C. M. Corbet, and E. Tutuc, *ACS Nano* **9**, 4527–4532 (2015).
- <sup>38</sup>M. Palummo, M. Bernardi, and J. C. Grossman, *Nano Lett.* **15**, 2794–2800 (2015).
- <sup>39</sup>C. Robert, D. Lagarde, F. Cadiz, G. Wang, B. Lassagne, T. Amand, A. Balocchi, P. Renucci, S. Tongay, B. Urbaszek, and X. Marie, *Phys. Rev. B* **93**, 205423 (2016).
- <sup>40</sup>G. Moody, J. Schaibley, and X. Xu, *J. Opt. Soc. Am. B* **33**, C39–C49 (2016).
- <sup>41</sup>W. Zhao, R. M. Ribeiro, and G. Eda, *Acc. Chem. Res.* **48**, 91–99 (2015).
- <sup>42</sup>M. M. Furchi, D. K. Polyushkin, A. Pospischil, and T. Mueller, *Nano Lett.* **14**, 6165–6170 (2014).
- <sup>43</sup>R. Yan, Q. Zhang, W. Li, I. Calizo, T. Shen, C. A. Richter, A. R. Hight-Walker, X. Liang, A. Seabaugh, D. Jena *et al.*, *Appl. Phys. Lett.* **101**, 022105 (2012).
- <sup>44</sup>C. Gong, H. Zhang, W. Wang, L. Colombo, R. M. Wallace, and K. Cho, *Appl. Phys. Lett.* **103**, 053513 (2013).
- <sup>45</sup>T. C. Berkelbach, M. S. Hybertsen, and D. R. Reichman, *Phys. Rev. B* **88**, 045318 (2013).
- <sup>46</sup>I. Kylänpää and H.-P. Komsa, *Phys. Rev. B* **92**, 205418 (2015).
- <sup>47</sup>M. Z. Mayers, T. C. Berkelbach, M. S. Hybertsen, and D. R. Reichman, *Phys. Rev. B* **92**, 161404 (2015).
- <sup>48</sup>D. K. Zhang, D. W. Kidd, and K. Varga, *Nano Lett.* **15**, 7002–7005 (2015).
- <sup>49</sup>T. Olsen, S. Latini, F. Rasmussen, and K. S. Thygesen, *Phys. Rev. Lett.* **116**, 056401 (2016).
- <sup>50</sup>J. P. Sun, G. I. Haddad, P. Mazumder, and J. N. Schulman, *Proc. IEEE* **86**, 641–660 (1998).
- <sup>51</sup>U. Chandni, K. Watanabe, T. Taniguchi, and J. P. Eisenstein, *Nano Lett.* **16**, 7982–7987 (2016).
- <sup>52</sup>Y. Wang, Z. Wang, W. Yao, G.-B. Liu, and H. Yu, *Phys. Rev. B* **95**, 115429 (2017).
- <sup>53</sup>K. Wang, B. Huang, M. Tian, F. Ceballos, M.-W. Lin, M. Mahjouri-Samani, A. Boulesbaa, A. A. Puzos, C. M. Rouleau, M. Yoon *et al.*, *ACS Nano* **10**, 6612–6622 (2016).
- <sup>54</sup>Q. Zheng, W. A. Saidi, Y. Xie, Z. Lan, O. V. Prezhdo, H. Petek, and J. Zhao, *Nano Lett.* **17**, 6435–6442 (2017).
- <sup>55</sup>H. Zhu, J. Wang, Z. Gong, Y. D. Kim, J. Hone, and X.-Y. Zhu, *Nano Lett.* **17**, 3591–3598 (2017).
- <sup>56</sup>B. Yang, E. Molina, J. Kim, D. Barroso, M. Lohmann, Y. Liu, Y. Xu, R. Wu, L. Bartels, K. Watanabe, T. Taniguchi, and J. Shi, *Nano Lett.* **18**, 3580–3585 (2018).